Neurosci. Bull. October, 2019, 35(5):826–840
https://doi.org/10.1007/s12264-019-00387-4

www.neurosci.cn
www.springer.com/12264

ORIGINAL ARTICLE

Modulation of Beta Oscillations for Implicit Motor Timing in Primate Sensorimotor Cortex during Movement Preparation

Hongji Sun[1,2] · Xuan Ma[2] · Liya Tang[3] · Jiuqi Han[2] · Yuwei Zhao[2] · Xuejiao Xu[2] · Lubin Wang[2] · Peng Zhang[2] · Luyao Chen[2] · Jin Zhou[2] · Changyong Wang[1,2]

Received: 14 October 2018 / Accepted: 9 December 2018 / Published online: 6 May 2019

Abstract Motor timing is an important part of sensorimotor control. Previous studies have shown that beta oscillations embody the process of temporal perception in explicit timing tasks. In contrast, studies focusing on beta oscillations in implicit timing tasks are lacking. In this study, we set up an implicit motor timing task and found a modulation pattern of beta oscillations with temporal perception during movement preparation. We trained two macaques in a repetitive visually-guided reach-to-grasp task with different holding intervals. Spikes and local field potentials were recorded from microelectrode arrays in the primary motor cortex, primary somatosensory cortex, and posterior parietal cortex. We analyzed the association between beta oscillations and temporal interval in fixed-duration experiments (500 ms as the Short Group and 1500 ms as the Long Group) and random-duration experiments (500 ms to 1500 ms). The results showed that the peak beta frequencies in both experiments ranged from 15 Hz to 25 Hz. The beta power was higher during the hold period than the movement (reach and grasp) period. Further, in the fixed-duration experiments, the mean power as well as the maximum rate of change of beta power in the first 300 ms were higher in the Short Group than in the Long Group when aligned with the Center Hit event. In contrast, in the random-duration experiments, the corresponding values showed no statistical differences among groups. The peak latency of beta power was shorter in the Short Group than in the Long Group in the fixed-duration experiments, while no consistent modulation pattern was found in the random-duration experiments. These results indicate that beta oscillations can modulate with temporal interval in their power mode. The synchronization period of beta power could reflect the cognitive set maintaining working memory of the temporal structure and attention.

Keywords Macaque · Primary motor cortex · Primary somatosensory cortex · Posterior parietal cortex · Temporal perception · Local field potentials

✉ Jin Zhou
sisun819@yahoo.com

✉ Changyong Wang
wcy2000_zm@163.com

[1] School of Life Science and Technology, Harbin Institute of Technology, 92 West Dazhi Street, Nan Gang District, Harbin 150080, China

[2] Department of Neural Engineering and Biological Interdisciplinary Studies, Institute of Military Cognition and Brain Sciences, Academy of Military Medical Sciences, 27 Taiping Rd, Beijing 100850, China

[3] Department of Neurology, Chinese PLA General Hospital, Beijing 100853, China

Introduction

Timing is involved in many aspects of behavior, manipulations ranging from microseconds to circadian rhythms that guide behavior in different ways [1–8]. Across diverse scales of temporal perception, interval timing at the level of hundreds of milliseconds is involved in activities such as speech comprehension, motion processing, and the coordination of fine movements. Patients suffering from diseases such as Parkinson's [9], Huntington's [10], dystonia [11], Tourette's syndrome [12], aphasia [13], attention-deficit/hyperactivity disorder [14], and schizophrenia [15] have difficulty in temporal perception over this time range.

Motor timing of several hundreds of milliseconds acts as an important part of the timing process. Imagine such

activities as crossing the road with the traffic signal, stopping your car before crashing into the car ahead, running after a visual go cue or hearing the starting guns and dancing to music. All the processes involved require using experience and environmental cues to anticipate the timing of a predictable event in order to perform properly. The motor timing process is divided into two main types: *explicit* and *implicit* timing [16]. During explicit timing tasks, the duration of the stimulus is always known before the estimation starts. This could be in the form of a discrimination task for certain intervals or a periodic motor act according to a certain beat. Conversely, in implicit timing studies, temporal expectation is performed discretely (not restricted to the temporal length) and is always used to perform better [17]. Studies on explicit timing have used both invasive and non-invasive methods, such as electrophysiological recording, electroencephalography, and magnetic resonance imaging to reveal that neural activity shows ramping [18, 19] of firing rates in different brain areas that include the prefrontal cortex [20], premotor cortex [21–23], primary motor cortex [24, 25], posterior parietal cortex [26, 27], and striatum [28]. In addition, neurons have been found to modulate their firing rates with explicit motor timing in the form of a small interconnected ensembles of neurons acting as a trigger for large neural activity [29–31], large populations of specific neurons acting as players in a dynamic state timing network [32–34], and circuit-specific neural activity form a general pattern for a timing network [29–31, 35, 36]. Reports have also shown that beta oscillations are modulated with different durations of beat perception [37–42], and auditory as well as motor cortical areas are both activated during auditory-motor timing perception tasks. While the same investigation methods have been used for implicit and explicit timing tasks, research has shown that ramping firing rates can also be used to decode different time intervals. Moreover, researchers have found that activated brain areas during implicit timing tasks are mainly located in the premotor, parietal cortex, and supramarginal gyrus of the left hemisphere [16, 43]. Despite recent developments in explicit and implicit timing research, studies focusing on the modulation of beta oscillations with implicit timing, which is thought to play an important role in the motor timing process, are scarce.

Inspired by previous studies on beat perception during explicit timing, which found correlations of beta oscillations with different rhythms, we designed experiments to investigate the relationship between beta oscillations and temporal perception during implicit motor timing for a further understanding of motor timing mechanism.

Materials and Methods

Subjects

Two adult monkeys (rhesus macaques, one male (Monkey B) and one female (Monkey D), both weighing $\sim$ 5.5 kg) were used in this study. All feeding, surgery, care, training, and experimental procedures were approved by the Institutional Animal Care and Use Committee of the Chinese Academy of Military Medical Science.

Experimental Apparatus

During the experiments, the monkeys were seated upright on a specially-designed primate chair [Fig. 1A (a)], with the head and left hand restrained (videos S1 and S2). An apparatus was designed for the reach-to-grasp task [Fig. 1A (a) and (c)]. A horizontal panel had a forced sensitive resistance (FSR) pad fixed in the center, 12 cm in front of the monkey, defined as the center pad [Fig. 1A (a) and (c)]. One green light-emitting diode (LED1) was positioned beside the center pad. On the vertical panel, a spherical target made by a 3D printer (Tiertime Inc., Beijing, China) was fixed centrally 6 cm above the horizontal panel. A green LED indicator (LED2) was placed beside the target [Fig. 1A (a) and (c)]. The Single-Chip Microcomputer (SCM) control component, mainly enabled communication between the upper monitor and the neural signal recording system, consisted of a power supply, electromagnetic control, LED control, event transmission, command transmission, and FSR control units [Fig. 1A (b)].

Training and Experimental Procedure

In the training period, each monkey was seated in the primate chair and the left hand was restrained by soft bands. The monkey's right hand was free to reach the target. The training period was divided into two stages. In stage 1, the monkey learned to hit the FSR pad on the horizontal panel and maintain pressure for a certain period to receive a water reward. During this period, the holding duration was gradually increased from 100 ms to 1500 ms. Once the success rate exceeded 90%, we moved to stage 2 training. In this stage, the monkey was taught to hold for 500 or 1500 ms before the Target On cue and then hit the spherical target in front of it and hold it for 200 ms to receive a water reward (Fig. 1B).

The different movement stages, separated by sequential event markers of Center Hit, Center Release, Target Hit, and Trial End were hold, reaction, reach, and grasp. As shown in Fig. 1C, we conducted two kinds of experiments:

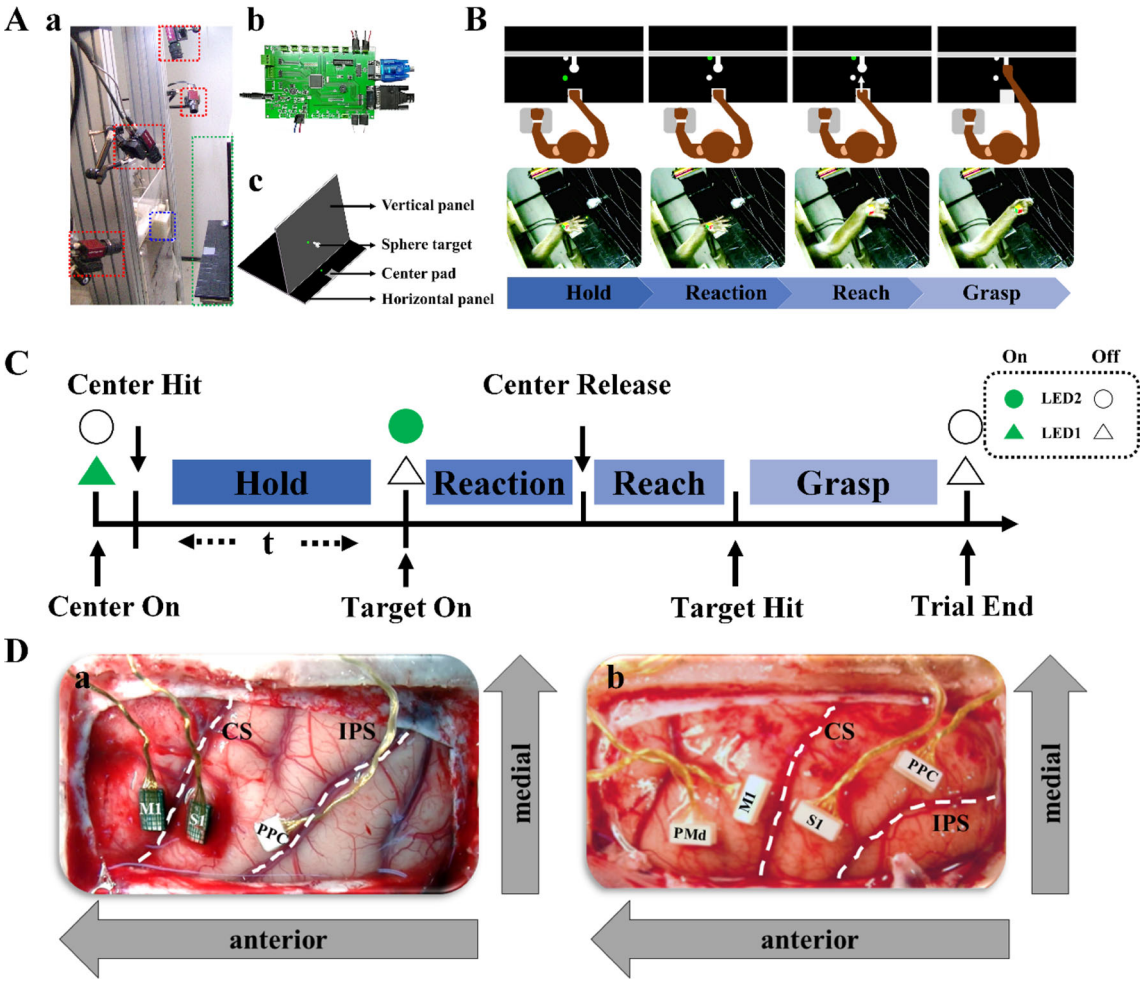

Fig. 1 Experimental procedure and electrode placement. **A** Experimental apparatus for the reach-to-grasp task. The setup consisted of a monkey chair, a fixation accessory for restraining the monkey's left hand (blue dashed square), four tracking cameras (red dashed squares), a reach-to-grasp apparatus (green dashed square) **(a** and **c),** and a Single-Chip Microcomputer (SCM) control unit for transmitting commands **(b)**. **B** Experimental paradigm for the reach-to-grasp task. The monkey's left hand was restrained by a soft band and its right hand was free to move following the relevant signals. **C** Sequence of events on a single trial. The experimental paradigm consisted of a hold epoch, followed by Target On cue, reaction, reach, and grasp epochs. Each trial began with the lighting of LED1 (Center On), which required the monkey to place its right hand on the pad (Center Hit, CH). When the time requirement had been satisfied, the target, LED2 on the vertical panel, was lit (Target On, TH). The monkey then reached toward the target object and grasped it (Target Hit, TH) for 200 ms before gaining a water reward. **D** Cortical locations of implanted microelectrodes. (**a**) For Monkey B, two 32-channel Utah arrays were implanted in cortical areas M1 and S1, and one 16-channel floating microelectrode array was placed in the PPC. (**b**) For Monkey D, four 32-channel floating microelectrode arrays were inserted into the PMd, M1, S1, and PPC. CS, central sulcus; IPS, intraparietal sulcus; PMd, dorsal premotor cortex; M1, primary motor cortex; S1, primary somatosensory cortex; PPC, posterior parietal cortex. White dashed lines indicate the locations of the CS and IPS (**a** and **b**).

trials with a fixed duration or a random duration of the holding period. In the fixed-duration experiments, we divided the trials into two groups according to the hold duration. Trials with a 500-ms holding time are referred to as the Short Group, while those with a 1500-ms holding time were the Long Group. With LED1 on, the monkey had to hit the center pad (Center Hit, CH) and maintain a fixed holding position for 500 ms or 1500 ms before LED2 came on (Target On, TO). The monkey then released its hand (Center Release, CR) to reach the spherical target (Target Hit, TH). The same experiment was conducted repetitively over three days for both monkeys with reach-to-grasp trials for the Short Group performed before trials for the Long Group. In the random-duration experiments, the duration of the holding period was random with a time ranging from 500 ms to 1500 ms. The other movements were the same as in the fixed-duration experiments.

Surgery

To explore electrophysiological features in the sensorimotor cortex during the different reach-to-grasp tasks,

electrodes were implanted under inhalation anesthesia (Isoflurane anesthesia, 1.5%) after the training procedures were completed. After implanting a holder, performing a craniectomy, opening the dura, and fixing a custom-made pedestal as in previous studies [44, 49], we identified the target areas by direct visual inspection of the central sulcus, arcuate sulcus, and superior precentral dimple and inserted the prepared electrodes [44–49]. For monkey B, two 32-channel Utah arrays were inserted into the primary motor cortex (M1) and primary somatosensory cortex (S1), and one floating 16-channel microelectrode array was placed in the posterior parietal cortex (PPC, area 5) [Fig. 1D (a)]. For monkey D, four floating microelectrode arrays were inserted into the dorsal premotor cortex (PMd), M1, S1, and PPC in sequence [Fig. 1D (b)]. The electrode array placed in the PMd was used in other studies. The dura was then sealed and covered with artificial dura and a bone fragment. A titanium mesh was fixed to the skull over the bone fragment before the skin was sutured. The monkeys were carefully rehabilitated after surgery. Essential antibiotics and analgesics were used during and after the surgery according to drug guidelines.

Recording Procedures and Data Acquisition

The monkeys were further trained in different reach-to-grasp tasks several weeks after surgery. Specifically, Monkeys B and D started training in the implicit timing task on days 270 and 107 after electrode placement, respectively. For the fixed-duration experiments, the monkeys were first trained for two days, then they performed the fixed-duration task on the following three consecutive days. The experimental order on each day consisted of trials with the short holding time (500 ms) performed first and then trials with the long holding time (1500 ms). During training and the repetitive reach-to-grasp tasks, the monkeys had already memorized the experimental order and formed a motor habit. In the random-duration experiments, the monkeys performed the reach-to-grasp task for four days (Monkey B) and six days (Monkey D). During the tasks, cortical neuronal activity was collected using OmniPlex-128, a 128-channel acquisition system (Plexon Inc., Dallas, TX, USA). The sampling rate for wide-band neural signals was 40 kHz per channel, down-sampled to 1 kHz for all local field potential (LFP) channels (each electrode channel provided one LFP dataset). Single and multi-unit activity were manually sorted offline using Offline Sorter (Plexon Inc.). Totals of 80 and 112 electrodes were selected for neural signal acquisition after excluding channels with high noise levels.

Data Analysis

Success Rate Analysis

The monkeys had to perform CH, CR, and TH and withhold from grasping the target sphere for 200 ms to get a reward. We defined a trial during which a monkey successfully accomplished CH, CR, and TH and received a water reward as a successful trial. The success rate (the number of successful trials divided by the total number of trials) was computed for trials performed in the fixed-duration and random-duration experiments.

Reaction Time Analysis

The reaction time was defined as the time from TO to CR. The reaction time of successful trials as well as the coefficient of variance (CV) in both the fixed- and random-duration experiments were analyzed.

LFP Analysis

After excluding channels with excessive noise during data acquisition, we recorded 80 channels of LFPs from Monkey B and 112 from Monkey D on each day. Further excluding abnormal channels, 78 remained for Monkey B (M1 31, S1 31, PPC 16) and 109 for Monkey D (PMd 32, M1 31, S1 21, PPC 25) for analysis. The LFPs from each electrode were filtered with a fourth-order Butterworth band-pass filter. Fluctuations in the low-frequency band and power supply noise were eliminated using the de-trending method based on local linear regression. The recorded LFP data from successful trials in the fixed- and random-duration experiments on different days were combined into four datasets for analysis. The first and second datasets were for the fixed-duration experiment. The first dataset was from Monkey B, and consisted of 78 channels of LFPs with 1546 trials in the Short Group and 1769 in the Long Group. For Monkey D, the second dataset consisted of 109 channels of LFPs from 775 trials in the Short Group and 582 in the Long Group. The third and fourth datasets were for the random-duration experiment. The third dataset was for Monkey B, and consisted of 78 channels of LFPs for 2670 successful trials. The fourth dataset was for Monkey D, and consisted of 109 channels of LFPs for 4130 successful trials. Trials in the random-duration experiment were divided into ten groups according to the holding duration for further analysis. The groups were as follows: group 1, 500–600 ms; group 2, 600–700 ms; group 3, 700–800 ms; group 4, 800–900 ms; group 5, 900–1000 ms; group 6, 1000–1100 ms; group 7, 1100–1200 ms; group 8, 1200–1300 ms; group 9,

1300–1400 ms; and group 10, 1400–1500 ms. The sampling rate of LFPs was set to 1000 Hz and only the power between 0.3 Hz and 100 Hz was used for analysis. The LFP data from M1, S1, and PPC were used for analysis. To explore the modulation of beta oscillations in implicit timing tasks, several methods, including spectrogram, peak frequency, and beta power analysis, were then applied.

Trial-Averaged Spectrogram Analysis

Beta power spectrograms were calculated using the multi-taper approach in the Chronux toolbox (http://chronux.org) [50]. The function used was mtspectrumc, with the parameters 1000 for Fs, [10 60] for fpass, 1 for trialave, 2 for pad, 2 for TW, and [2 3] for tapers. A 200-ms wide window with a sliding length of 10 ms was used for power estimation, and the time-bandwidth was set to 2 Hz. In this analysis, the beta band was defined as 13 Hz–30 Hz. The calculated results were averaged for all the trials of the same condition. The time windows shown in the spectrogram figures were 1000 ms for the Short Group and 1800 ms for the Long Group. The aligned event was Center Hit for both groups. The beta power spectral changes of an arbitrary channel in M1, S1, and PPC for the Short and Long Groups are shown as examples in Fig. 2.

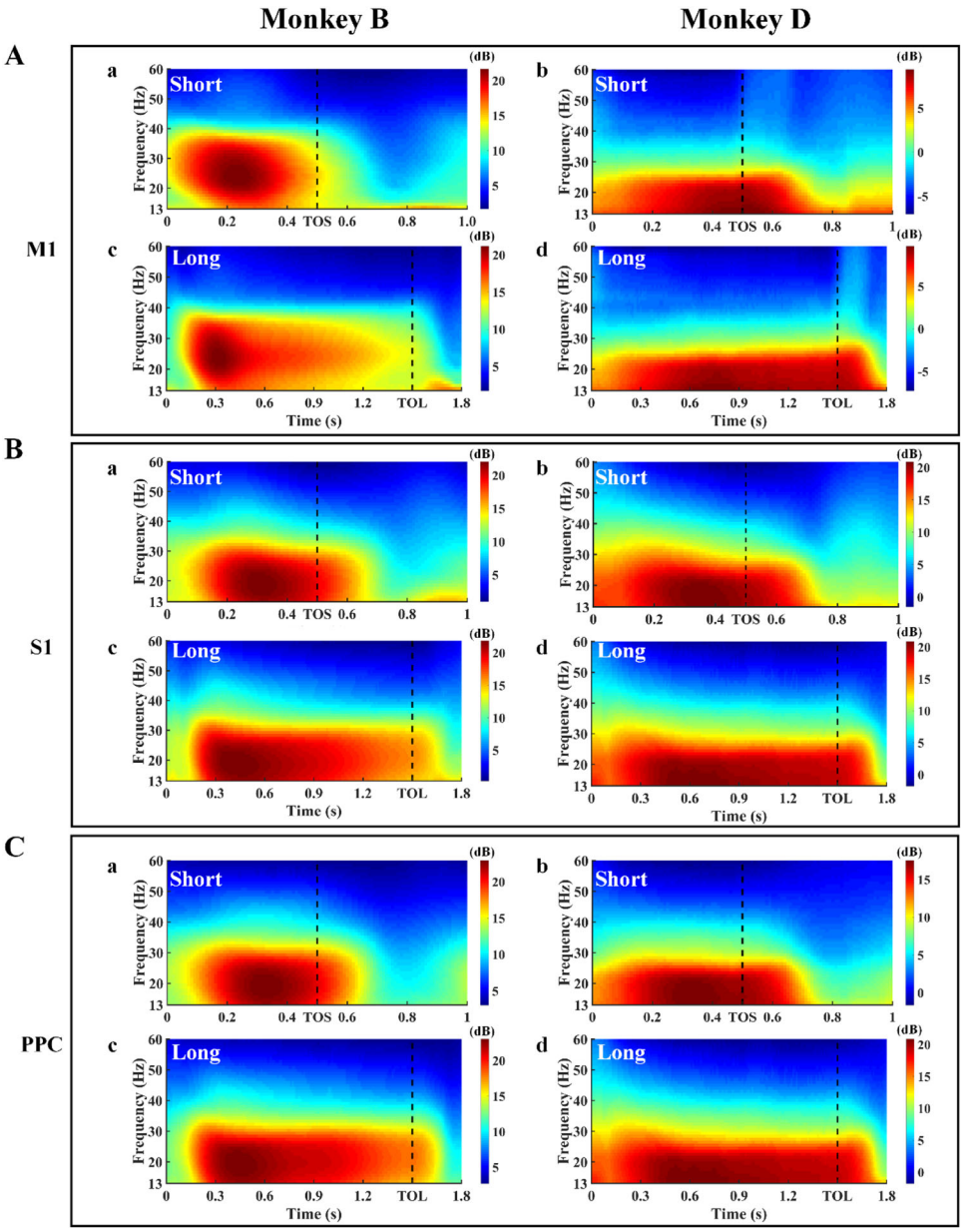

Fig. 2 Trial-averaged spectrograms of LFP signals from M1 (**A**), S1 (**B**) and PPC (**C**) in Monkey B (left) and Monkey D (right) aligned on Center Hit. The data from an arbitrary channel in M1, S1, and PPC are shown in **A** (a, c), **B** (a, c), and **C** (a, c) for Monkey B and **A** (b, d), **B** (b, d), and **C** (b, d) for Monkey D. In all cases, (a) and (b) are from the Short Group tasks, while (c) and (d) are from the Long Group tasks. The black vertical dashed lines indicate the Target On event (TOS, Target On of the Short Group; TOL, Target On of the Long Group). The color bar indicates the absolute values of the beta power spectra.

Analysis of Context-Related Frequency Modulation of Beta Oscillation

The peak frequency of beta power was then analyzed, also using mtspectrumc. The parameters were set to 1000 for Fs, [13 30] for fpss, 1 for trialave, [1 0.05] for err, 1 for pad, 5 for TW, and [5 9] for tapers. The beta power was smoothed by a 10-Hz window using the smooth function in MatLab. The peak beta frequency of each electrode was computed by locating the frequency of the maximum beta power using MatLab.

Analysis of Beta Power

We computed the mean beta power spectra around the peak beta frequencies that ranged from 15 Hz to 25 Hz, still using mtspectrumc. The parameters were set to the same values as those for the trial-averaged spectrogram. The beta power in different groups was computed and smoothed with a 10-Hz window using the smooth function in MatLab. To compare the results from different groups in the same brain area for each monkey, the beta power in an area was normalized by dividing by the maximum mean value. The beta power change over time during the holding period in M1, S1, and PPC for the fixed- and random-duration experiments are shown in Figs. 3 and 4. The beta power in different movement stages (hold, reaction, reach, and grasp) for each brain area was analyzed using one-way ANOVA testing (Fig. 5). The synchronization period (the rising phase of the beta power change) was located. The overlap was $\sim$ 300 ms, the focus period for beta oscillation analysis. The mean beta power in the first 300 ms (BP) and the peak latency of the maximum beta power during the holding period (PLB), as well as the maximum rate of change of beta power during the first 300 ms (MSB) for both individual channels and the overall performance in each brain area (Figs. 6, 7, and 8) were then compared using the Mann-Whiney U test for the fixed-duration experiments and one-way ANOVA for the random-duration experiments. The statistical significance level was set to 0.05. For the random-duration experiments, BP, PLB, and MSB were analyzed among 10 groups.

Results

Behavioral Performance

In the fixed-duration experiments, a total of 3485 trials were accomplished by monkey B and 1434 by monkey D, and in the random-duration experiments, 2975 trials were accomplished by Monkey B and 4392 by Monkey D. We further analyzed the success rates and reaction times to assess task performance.

Success Rate

In the fixed-duration experiments, Monkey B completed totals of 1546 and 1769 successful trials, while monkey D accomplished 775 and 582 successful trials for the Short and Long group tasks, respectively. The success rates for monkey B were 93.92% for the Short Group and 96.19% for the Long Group, and the corresponding rates for monkey D were 94.74% and 94.48%. In the random-duration experiments, 2670 successful trials were accomplished by Monkey B and 4130 by Monkey D. The corresponding success rates were 89.75% and 94.03%.

Reaction Time

In the fixed-duration experiments, the reaction times for the Short and Long Groups were 198.20 ± 95.48 and 214.50 ± 67.07 ms for Monkey B; and 155.40 ± 80.90 and 219.00 ± 61.30 ms for Monkey D. In the random-duration experiments, the reaction times were 182.70 ± 39.08 ms for Monkey B and 180.90 ± 28.88 ms for Monkey D. Further analysis of the variation of reaction times by coefficient of variation (CV) analysis revealed CVs of 0.48, 0.31, and 0.21 for the Short, Long, and Random Groups for Monkey B, and 0.52, 0.28, and 0.16 for Monkey D.

Beta Oscillation Changes in M1, S1, and PPC

A total of 80 channels of LFPs were identified for Monkey B and 112 for Monkey D. We selected 78 LFPs from Monkey B and 77 from Monkey D for further analysis of beta oscillations in M1, S1, and PPC. The remaining LFPs were excluded because of artifacts detected by visual inspection.

Time–frequency Maps of Beta Power Spectra

To obtain a general picture of how beta power changed over time in different channels, we analyzed the beta power spectra of the LFPs in each electrode channel (M1, S1, and PPC) using the mtspectrumc function in the Chronux toolbox. The beta power spectra of different channels in the same brain area were similar during the holding period, so we chose an arbitrary channel for each area as an example to show the general change of spectra. The spectra of M1 [Fig. 2A (a) and (c)], S1 [Fig. 2B (a) and (c)], and PPC [Fig. 2C (a) and (c)] for Monkey B and M1 [Fig. 2A (b) and (d)], S1 [Fig. 2B (b) and (d)], and PPC [Fig. 2C (b) and (d)] for Monkey D showed that the trial-averaged

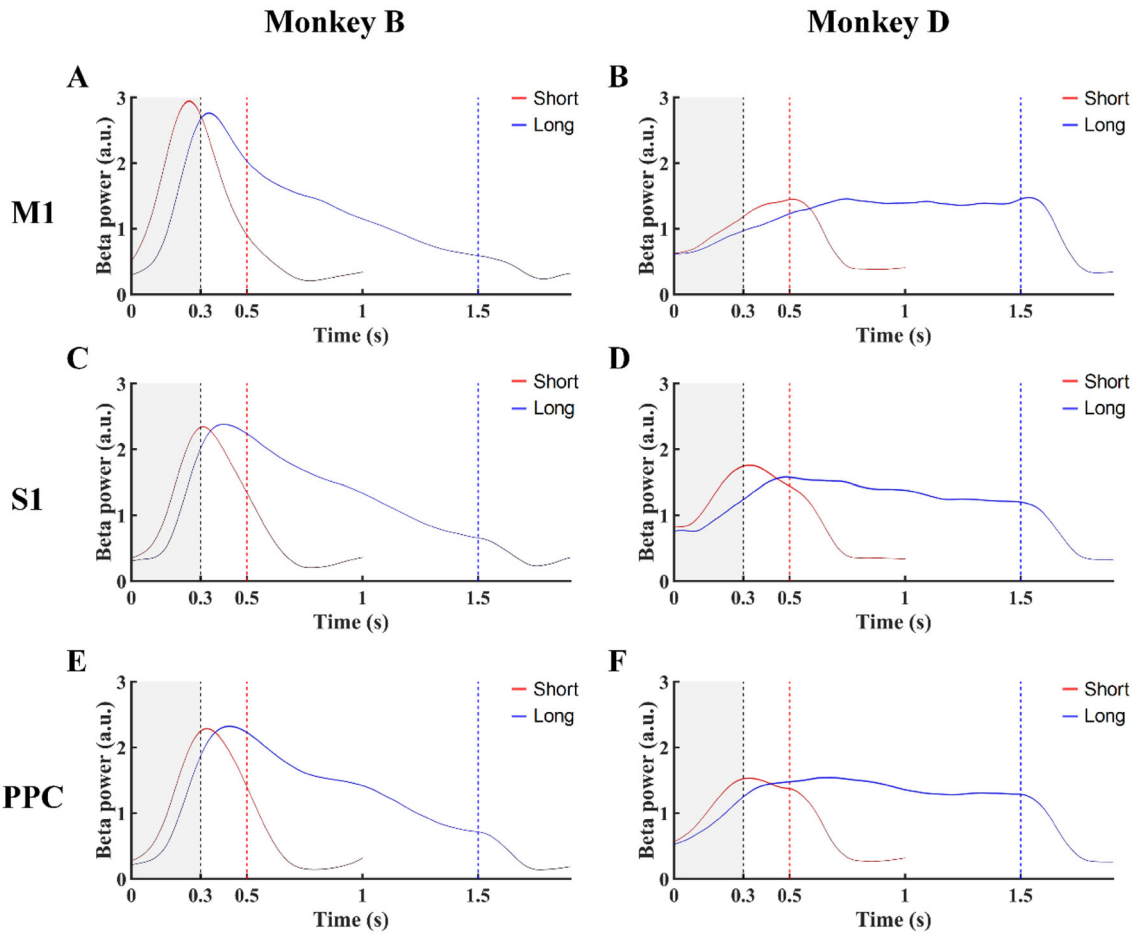

Fig. 3 Beta power changes over time in M1, S1, and PPC for Monkey B (**A**, **C**, **E**) and Monkey D (**B**, **D**, **F**) in the fixed-duration mode. Red lines, Short Group tasks; blue lines, Long Group tasks; black dashed lines, end of the 300-ms window (gray) from CH (0 on x axis); red and blue dashed lines, onset times of TO for the Short Group, and Long Group, respectively.

beta power spectra were higher prior to the Target On cue, which served as a go signal. Further, the highest components of spectra were in the holding period before TO for both the Short and Long Groups, independent of brain areas and subjects.

Context-Related Frequency Modulation in M1, S1, and PPC

To ascertain which frequency contributes most to the spectral power of the broad-band beta frequency, we conducted peak analysis of the beta band frequency for each channel using the mtspectrumc function. In the fixed-duration experiments, the peak frequencies for M1, S1, and PPC were 22.75 ± 3.54, 20.95 ± 3.89, and 20.69 ± 3.96 Hz for the Short Group and 22.89 ± 3.53, 21.81 ± 3.77, and 21.58 ± 3.93 Hz for the Long Group in Monkey B. The corresponding values in Monkey D were 19.50 ± 3.46, 19.95 ± 3.48, and 18.94 ± 3.58 Hz for the Short Group and 19.72 ± 3.45, 20.39 ± 3.44, and 19.30 ± 3.53 Hz for the Long Group, respectively. In the random-duration experiments, these values were 21.22 ± 3.72, 21.06 ± 3.88, and 20.55 ± 3.96 Hz in Monkey B and 20.16 ± 3.68, 20.84 ± 3.54, and 19.81 ± 3.61 Hz in Monkey D. We found that the peak frequencies of the power spectra were in the beta band range from 15 Hz to 25 Hz for both experiments in all three brain areas.

Beta Power in M1, S1, and PPC

We then analyzed the beta power around the peak frequency (15–25 Hz), to assess changes during different movement stages. Using beta power analysis, we obtained the absolute beta power of individual electrode channels and plotted the mean change in each brain area (Figs. 3, 4). The beta power showed an increasing pattern to the peak before a decreasing pattern, consistent with previous studies [51, 52].

To further understand how beta power changed during different movement stages, we used the event markers of

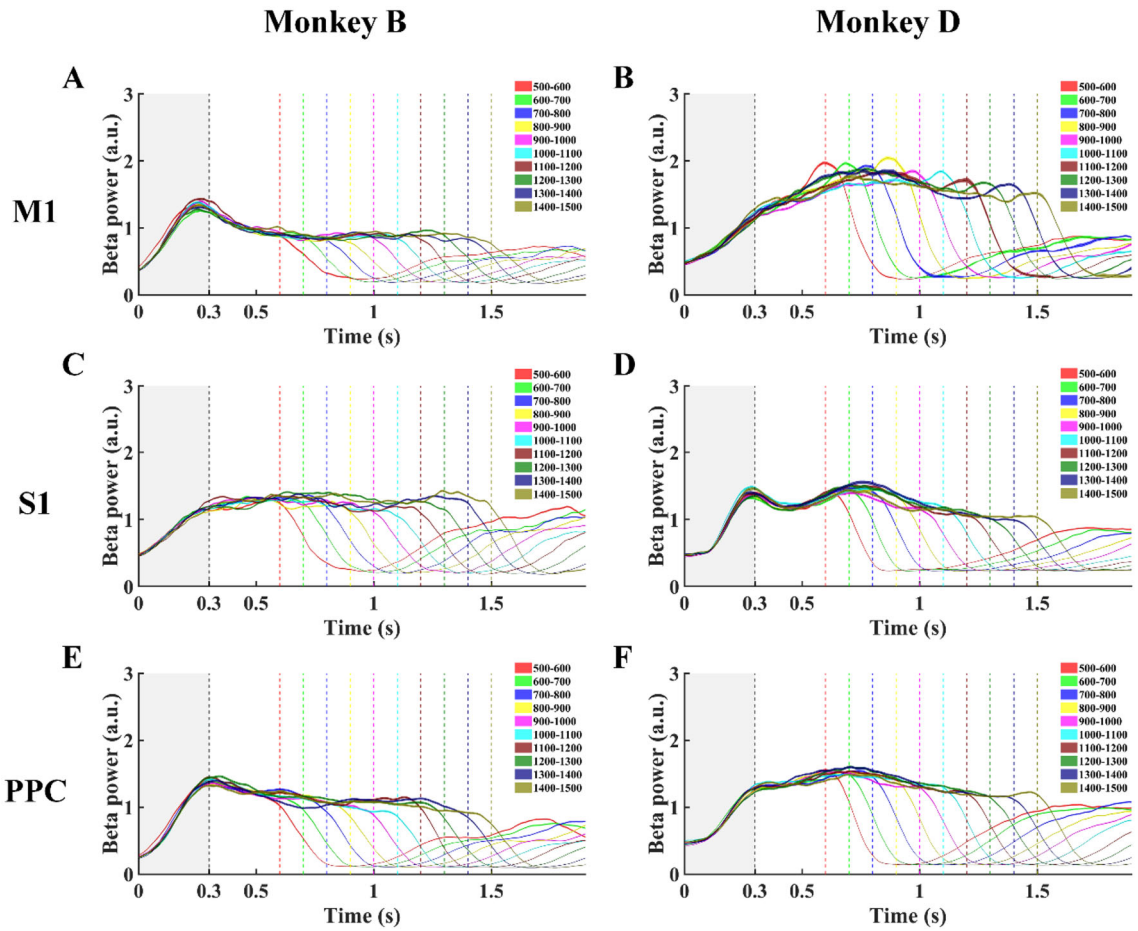

Fig. 4 Beta power changes over time in M1, S1, and PPC for Monkey B **(A, C, E)** and Monkey D **(B, D, F)** in the random-duration mode. Power changes of ten groups with different hold durations are shown. Dashed vertical lines from left to right are end of the 300-ms window (gray) from CH (0 on x axis) and each of ten Target On events.

CH, TO, CR, and TH to analyze beta power in the movement stages hold, reaction, reach, and grasp (Fig. 5). Compared with the hold period, the power in different brain areas in both the fixed- and the random-duration experiments was lower in the reach and grasp periods ($P < 0.05$, one-way ANOVA).

To further explore the characteristics of the changes in beta power, we focused on the rising phase, which is considered to be beta synchronization related to attention, anticipation, and working memory. We analyzed three parameters: mean beta power in the first 300 ms (BP), peak latency of the maximum power during the holding period (PLB), and the maximum rate of change of power within the first 300-ms window (MSB), and compared the results from different experiments. In the fixed-duration experiment, the normalized BPs for M1, S1, and PPC were 1.90 ± 0.01, 1.15 ± 0.01, and 1.07 ± 0.01 in the Short Group and 1.14 ± 0.01, 0.77 ± 0.11, and 0.71 ± 0.01 in the Long Group in Monkey B (Fig. 6A); and the corresponding values were 0.85 ± 0.01, 1.21 ± 0.01, and 1.04 ± 0.01 for the Short Group and 0.75 ± 0.01, 0.91 ± 0.01 and 0.82 ± 0.01 for the Long Group in Monkey D (Fig. 6B). The BPs values from the three brain areas were higher in the Short Group than in the Long Group ($P < 0.05$, Mann-Whiney U test) (Fig. 6A, B). The MSB values for M1, S1, and PPC were 49.75 ± 0.31, 29.70 ± 0.12, and 27.05 ± 0.16 for the Short Group and 36.32 ± 0.20, 24.85 ± 0.10, and 22.30 ± 0.13 for the Long Group in Monkey B (Fig. 6E); and 16.54 ± 0.08, 22.73 ± 0.17, and 18.73 ± 0.12 for the Short Group and 14.76 ± 0.08, 16.94 ± 0.13, and 16.02 ± 0.11 for the Long Group in Monkey D (Fig. 6F). Similar to BPs, the MSB values in the three brain areas were higher in the Short Group than in the Long Group ($P < 0.05$, Mann-Whiney U test). Further, the PLB values were 290.75 ± 0.62, 340.84 ± 0.56, and 351.14 ± 0.82 ms for the Short Group and 504.28 ± 0.96, 553.92 ± 0.94, and 577.29 ± 1.35 ms for the Long Group in M1, S1, and PPC in Monkey B (Fig. 6C); and 427.66 ± 1.18, 355.17 ± 1.36, and 372.55 ± 1.22 ms for the Short Group

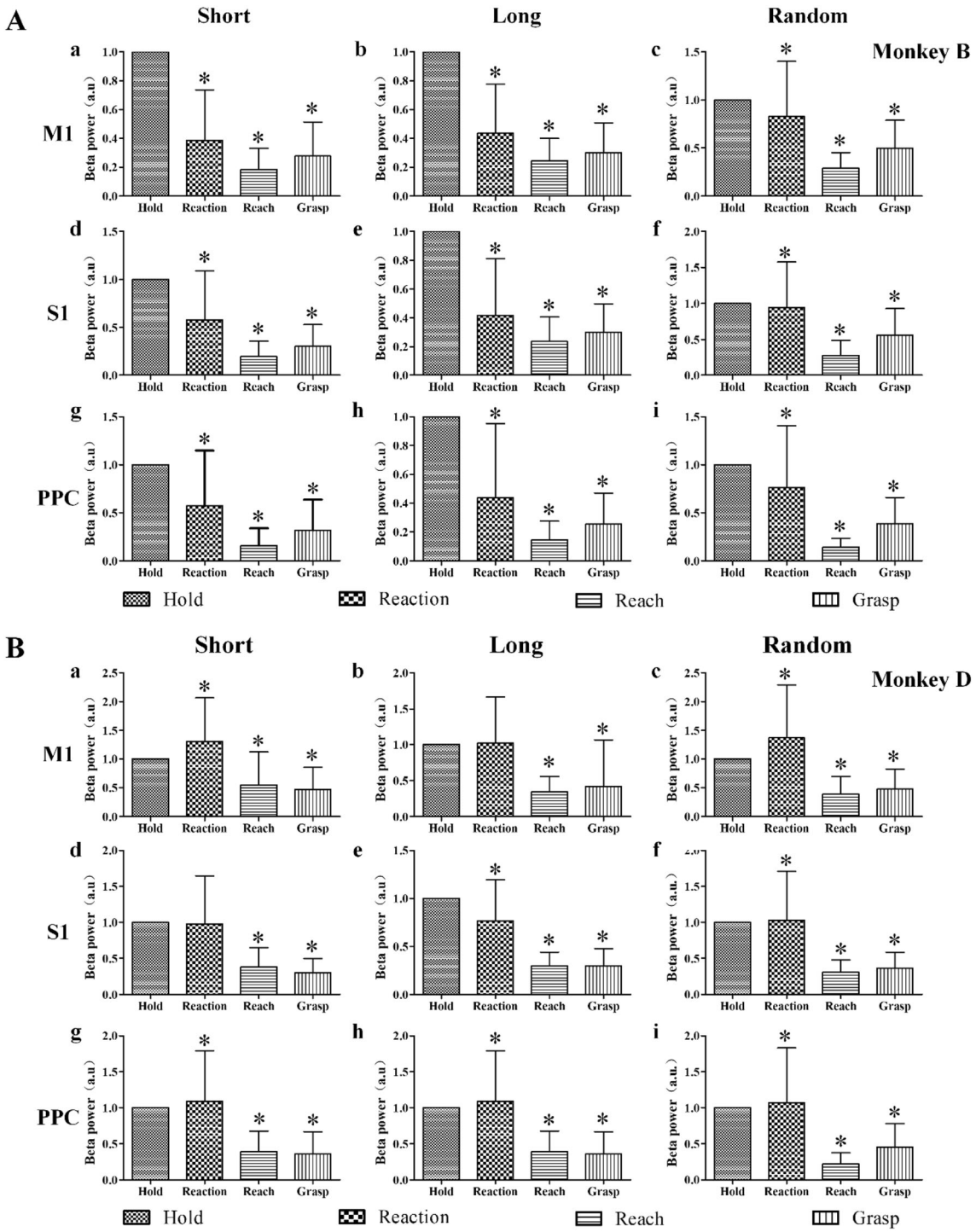

Fig. 5 Beta power in different movement stages for M1 (**a**–**c**), S1 (**d**–**f**), and PPC (**g**–**i**) in Monkey B (**A**) and Monkey D (**B**). Left column, fixed-duration in the Short Group; middle column, fixed-duration in the Long Group; right column, random-duration experiments; $*P < 0.05$ compared with the hold period, one-way ANOVA.

and 658.82 ± 1.93, 584.36 ± 2.42, and 618.27 ± 2.16 ms for the Long Group in Monkey D (Fig. 6D). The peak beta power appeared earlier than the Target On event in both groups, consistent with previous studies [51, 52]. Comparing the groups, the PLB during the holding period in the three brain areas was shorter in the Short Group than in the Long Group ($P < 0.05$, Mann-Whiney U test) (Fig. 6C, D). In addition, we analyzed BP, MSB, and PLB

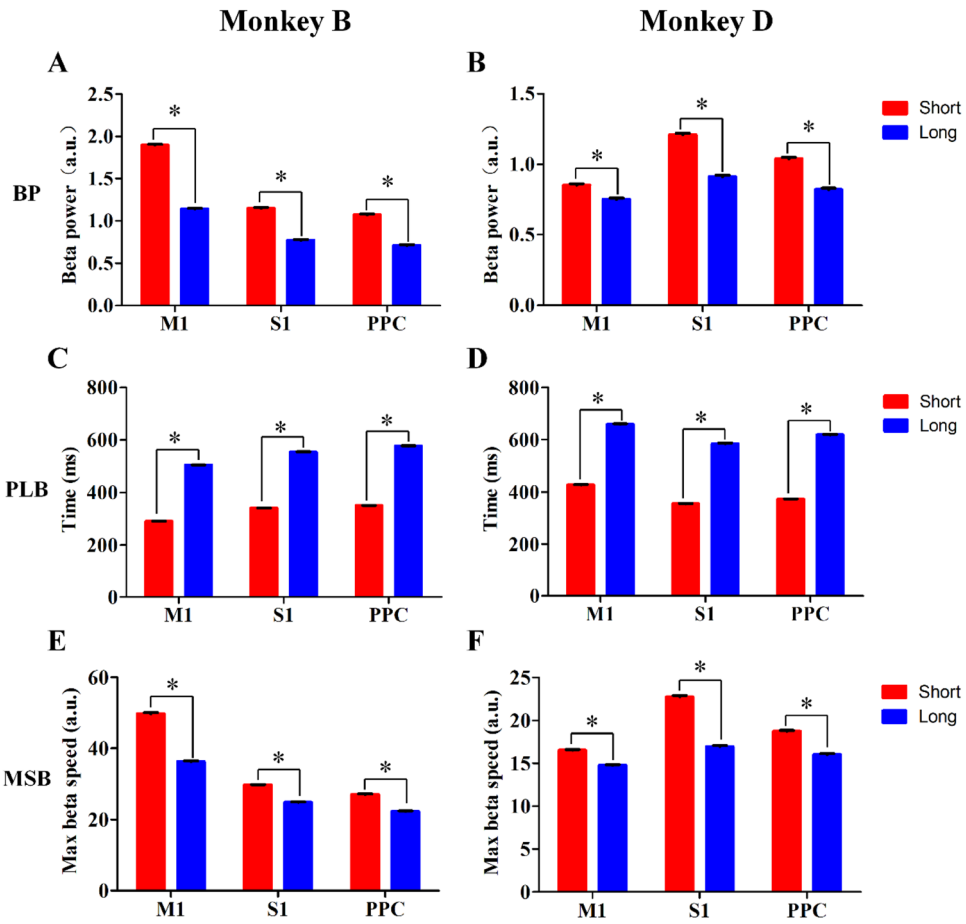

Fig. 6 Beta power modulation in M1, S1, and PPC in the fixed-duration experiments. Mean beta power during the first 300-ms window (BP), peak latency of maximum beta power during the holding period (PLB), and maximum rate of change of beta power during the first 300-ms window (MSB) in the Short Group (red bars) and the Long Group (blue bars) in Monkey B (**A**, **C**, **E**) and Monkey D (**B**, **D**, **F**). *$P < 0.05$, Mann–Whiney U test.

for individual channels and computed the percentages of channels with the same modulation pattern as its brain area. The percentages of PB and MSB in M1, S1, and PPC were all 100% for Monkey B and 93.55%, 100%, and 100% for Monkey D, respectively. For PLB during the holding period, the percentages were 100% for all the brain areas in both monkeys. We concluded that the modulation patterns of BP, MSB, and PLB are useful in differentiating the Short and Long Groups, and could represent the temporal structure in individual subjects.

In the random-duration experiments, the BP and MSB values showed no statistical difference between groups (Fig. 7, $P > 0.05$, one-way ANOVA), and the PLB in different brain areas did not show as consistent a modulation pattern as in the fixed-duration experiments (Fig. 8). The percentages showed a similar modulation pattern as its brain areas for BP, PLB, and MSB were 100% for S1 and PPC in Monkey B, and the corresponding values for M1 were 100%, 83.87% and 100%. In Monkey D, the percentages for PPC were all 100%; the corresponding values for M1 were 80.65%, 100%, and 96.77%; and for S1, were 100%, 95.24%, and 100%.

Discussion

In this study, each monkey was required to keep its hand still for different times before reaching to grasp a specific target in response to a visually-guided go cue. According to the functional definition of motor timing, the process in this task is of the implicit timing type [16]. With precise estimation of temporal intervals, the monkey could react better and thus obtain more rewards [53].

According to previous studies of beta oscillations, beat-based sound-induced beta power in the auditory cortex increases before the next beat and shows no phase-locking to sensory or motor events in explicit timing tasks [38]. Moreover, another report has shown that beta power differed between short- and long-delay trials in the primary motor cortex in the delay period before a visual go cue for one of two subjects in implicit timing tasks [51]. Both findings suggest that beta power is modulated with different temporal intervals. In our experiments, we found higher beta power during the holding period than the reach and grasp periods across different brain areas (M1, S1, and PPC), consistent with the results of previous studies

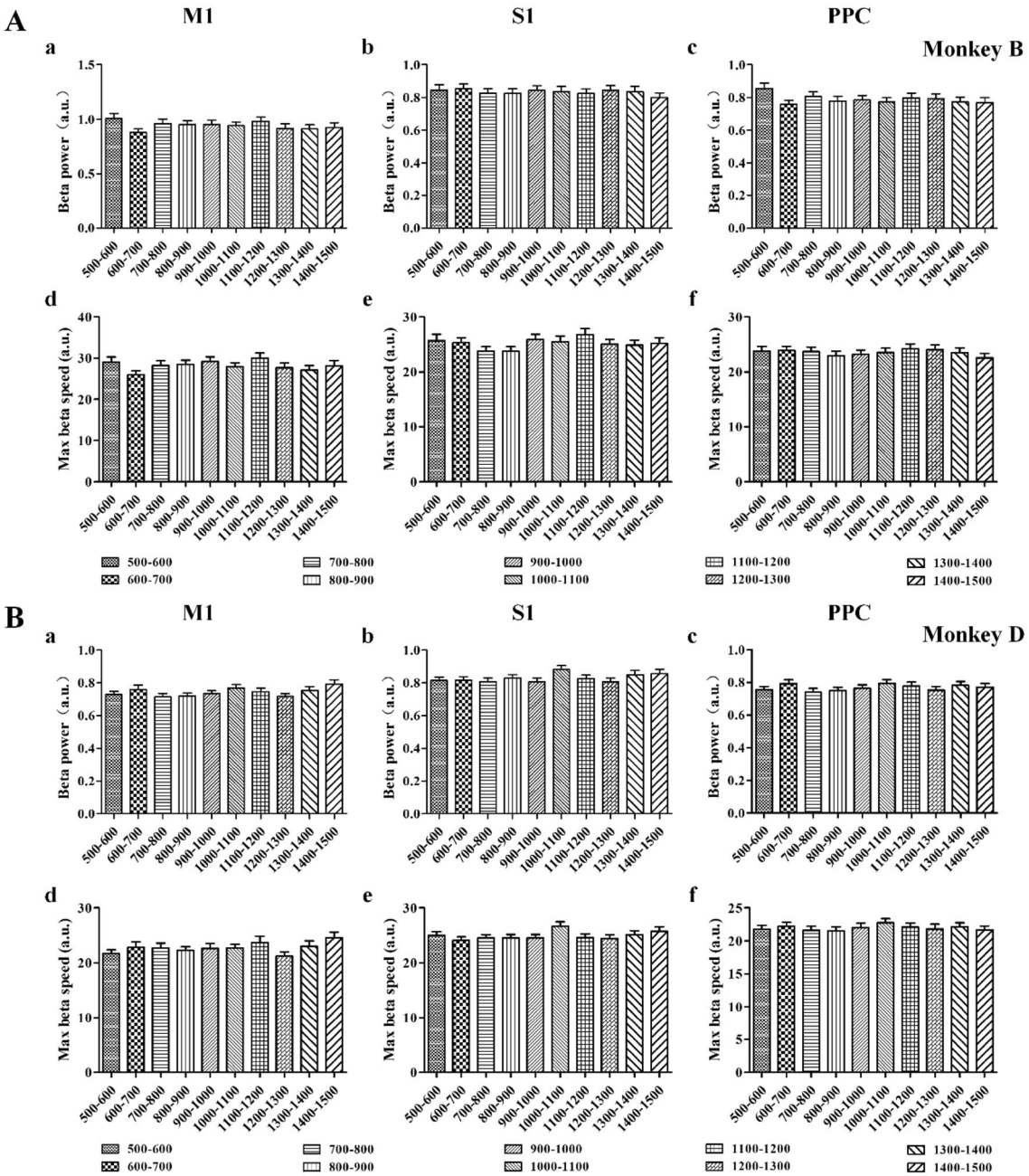

Fig. 7 Beta power modulation of BP (**a**–**c**) and MSB (**d**–**f**) in M1 (left column), S1 (middle column), and PPC (right column) for Monkey B (**A**) and Monkey D (**B**). Values for ten groups are aligned from left to right (mean ± SD). BP and MSB both showed no statistical difference between groups for different brain areas ($P > 0.05$, one-way ANOVA).

[51, 52]. Furthermore, in the fixed-duration experiments, we found that the BP and MSB during the beta power synchronization period were higher with a short interval than with a long interval. Meanwhile, the PLB during the holding period for a short interval was shorter than that for a long interval, while in the random-duration experiments, the PB and MSB showed no statistical difference. Further, the PLB showed a different modulation pattern in each brain area.

How does beta power synchronization modulate with different temporal intervals in implicit timing tasks? Unlike beta power desynchronization, which signifies motor preparation, movement execution, and motor imagery [54–57], synchronization has been suggested to be correlated with attention [58, 59], working memory [60, 61], and top-down motor expectation [40]. During explicit timing tasks, beta oscillations have been proposed for the top-down motor expectation signal of the beat structure in the

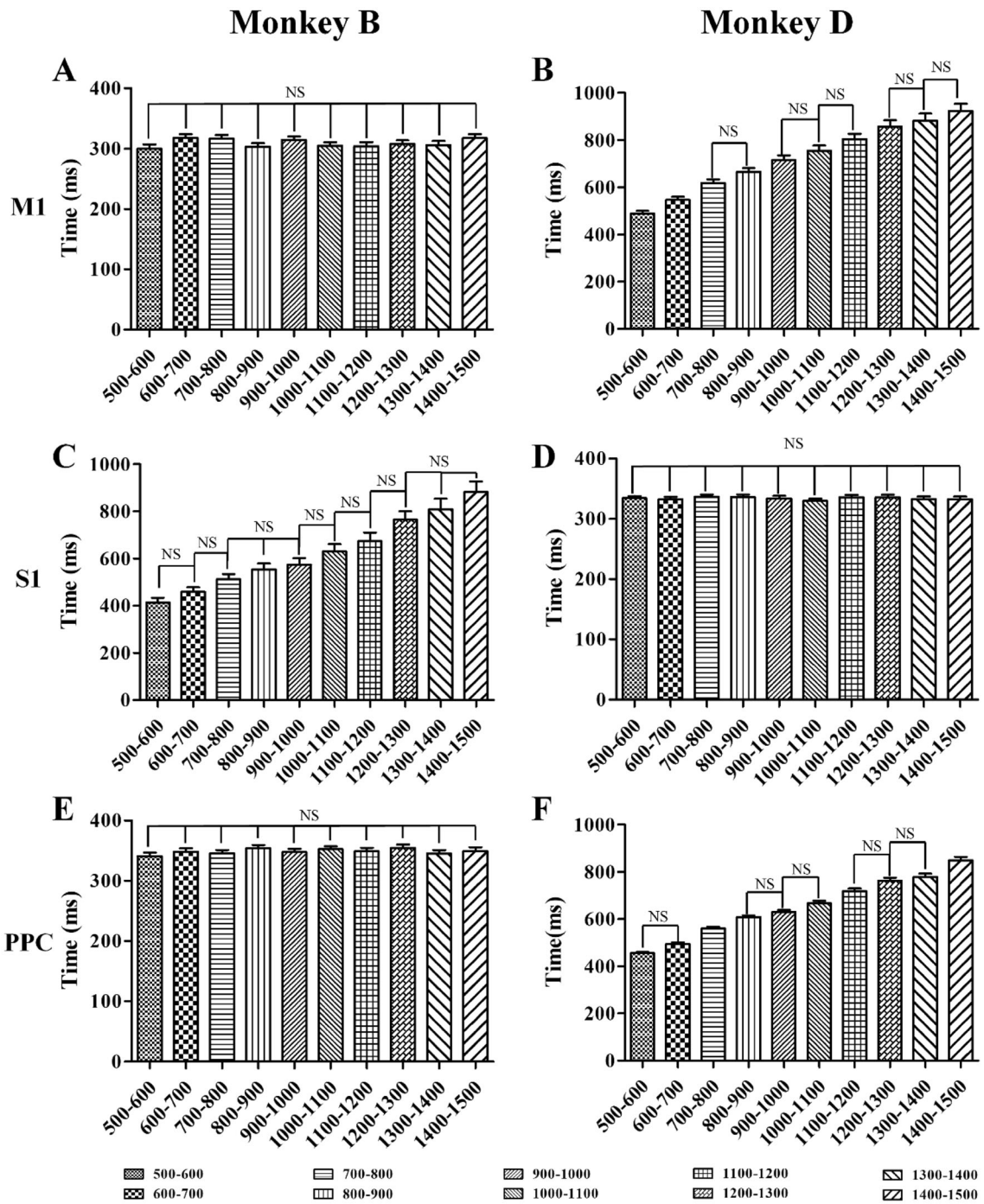

Fig. 8 Beta power modulation of PLB in M1 (**A**, **B**), S1 (**C**, **D**), and PPC (**E**, **F**) for Monkey B (left column) and Monkey D (right column). PLB values for ten groups are aligned from left to right (mean ± SD). The PLB of M1 and PPC in Monkey B as well as S1 in Monkey D showed no statistical difference between groups; NS, no significant difference, one-way ANOVA.

auditory system [40] and top-down control of internally-driven isochronous tapping [62]. Our implicit timing experiments showed that beta oscillations are modulated with the temporal intervals during the task. In a task that requires the subject to perform repetitive reach-to-grasp, the subject may have already remembered the general pattern of the task, such as experimental order and the length of the temporal intervals during the holding period, forming a motor habit that is correlated with the working memory of the task procedure and its temporal structure. Conversely, in the random-duration experiment, the temporal duration is impossible to anticipate accurately. The monkeys could neglect the temporal structure and focus more on the following instructions to perform better. The

variability of the reaction time (CV) was smaller in the random-duration experiments than in the fixed-duration experiments. We therefore suggest that the modulation pattern of beta power synchronization maintained the cognitive set for working memory of the temporal structure in the fixed-duration experiments and for attention in the random-duration experiments. Working memory is the short-term storage of information for later goal-directed action [63]. During previous studies, researchers found that beta oscillations are correlated with working memory both in the prefrontal and sensorimotor cortex [64–73]. Further, the *status quo*-maintaining hypothesis suggests that beta oscillations are part of a mechanism engaged in maintaining the *status quo* across large portions of the motor system [74]. The *status quo* could be the maintenance of the current motor set or continuation of the cognitive set. Our results for beta power modulation support this hypothesis. In the tasks in this study, the monkeys could have already remembered the temporal length and the experimental event sequence in which they would perform hundreds of repetitive short-duration trials and then long-duration trials in the fixed-duration experiments. Moreover, with the guide of each trial's start signal, the visual go cue could also be estimated in the realm of working memory of the temporal structure. The synchronization period of beta power, to some extent, represents the retrieval process of such working memory. Specifically, the time of occurrence of peak beta power could represent the monkey's working memory of the temporal length, whereas in the random-duration experiments, the modulation of beta power could reflect the maintenance of attention.

In conclusion, a reach-to-grasp implicit timing task was established and a modulation pattern of beta oscillation with temporal perception was found; that is, the power mode of beta oscillations can reflect the maintenance of cognitive set. Beta power modulation in the synchronization period could reflect the maintenance of the *status quo* of working memory for the temporal structure during movement preparation in the fixed-duration experiments, and attention for the following task procedure. The results showed how beta oscillations modulate with different temporal intervals in the implicit timing task, which provides new insight for future studies of implicit timing during different movements, and therefore aid our understanding of the mechanisms underlying motor timing. In future work, a more sophisticated paradigm is needed to conduct combined research involving compound muscle action potentials, spikes, and LFPs in different brain areas such as the prefrontal cortex, visual cortex, hippocampus, and striatum using functional magnetic resonance imaging (fMRI), electrophysiological recording, and optogenetics. Functional changes in different brain areas can be acquired using fMRI, which can guide further research with electrophysiological recording. Using electrophysiological recording techniques and optogenetics, specific neuronal types can be manipulated to obtain information about the function of a certain neuronal type. In addition, information flow between different brain areas and brain-muscle interactions can be assessed using brain network analysis [75, 76], coherence analysis [50], and Granger causal analysis [77, 78].

Acknowledgements This work was supported by the International Cooperation and Exchange of the National Natural Science Foundation of China (31320103914), the General Program of the National Natural Science Foundation of China (31370987), the National Natural Science Foundation of China for Outstanding Young Scholars (81622027), the Beijing Nova Program of China (2016B615), and the National Basic Research Development Program of China (2017YFA0106100).

Conflict of interest The authors claim that there are no conflicts of interest.

References

1. Merchant H, Harrington DL, Meck WH. Neural basis of the perception and estimation of time. Annu Rev Neurosci 2013, 36: 313–336.
2. Heys JG, Dombeck DA. Evidence for a subcircuit in medial entorhinal cortex representing elapsed time during immobility. Nat Neurosci 2018, 21: 1574–1582.
3. Bortoletto M, Cook A, Cunnington R. Motor timing and the preparation for sequential actions. Brain Cogn 2011, 75: 196–204.
4. Sohn MH, Carlson RA. Implicit temporal tuning of working memory strategy during cognitive skill acquisition. Am J Psychol 2003, 116: 239–256.
5. Gallistel CR, Gibbon J. Time, rate, and conditioning. Psychol Rev 2000, 107: 289–344.
6. Barclay JL, Tsang AH, Oster H. Interaction of central and peripheral clocks in physiological regulation. Prog Brain Res 2012, 199: 163–181.
7. Mohawk JA, Green CB, Takahashi JS. Central and peripheral circadian clocks in mammals. Annu Rev Neurosci 2012, 35: 445–462.
8. Li S, Wang Y, Wang F, Hu LF, Liu CF. A new perspective for Parkinson's disease: circadian rhythm. Neurosci Bull 2017, 33: 62–72.
9. de Hemptinne C, Ivanoiu A, Lefèvre P, Missal M. How does Parkinson's disease and aging affect temporal expectation and the implicit timing of eye movements? Neuropsychologia 2013, 51: 340–348.
10. Tabrizi SJ, Langbehn DR, Leavitt BR, Roos RA, Durr A, Craufurd D, *et al.* Biological and clinical manifestations of Huntington's disease in the longitudinal TRACK-HD study: cross-sectional analysis of baseline data. Lancet Neurol 2009, 8: 791–801.
11. Martino D, Lagravinese G, Pelosin E, Chaudhuri RK, Vicario CM, Abbruzzese G, *et al.* Temporal processing of perceived body movement in cervical dystonia. Mov Disord 2015, 30: 1005–1007.
12. Vicario CM, Gulisano M, Martino D, Rizzo R. Timing recalibration in childhood Tourette syndrome associated with persistent pimozide treatment. J Neuropsychol 2016, 10: 211–222.

13. Stein J, Walsh V. To see but not to read; the magnocellular theory of dyslexia. Trends Neurosci 1997, 20: 147–152.
14. Toplak ME, Tannock R. Time perception: modality and duration effects in attention-deficit/hyperactivity disorder (ADHD). J Abnorm Child Psychol 2005, 33: 639–654.
15. Penney TB, Meck WH, Roberts SA, Gibbon J, Erlenmeyer-Kimling L. Interval-timing deficits in individuals at high risk for schizophrenia. Brain Cogn 2005, 58: 109–118.
16. Coull J, Nobre A. Dissociating explicit timing from temporal expectation with fMRI. Curr Opin Neurobiol 2008, 18: 137–144.
17. Grahn JA, Brett M. Rhythm and beat perception in motor areas of the brain. J Cogn Neurosci 2007, 19: 893–906.
18. Merchant H, Zarco W, Perez O, Prado L, Bartolo R. Measuring time with different neural chronometers during a synchronization-continuation task. Proc Natl Acad Sci USA 2011, 108: 19784–19789.
19. Merchant H, Bartolo R. Primate beta oscillations and rhythmic behaviors. J Neural Transm (Vienna) 2018,125:461–470.
20. Brody CD, Hernández A, Zainos A, Romo R. Timing and neural encoding of somatosensory parametric working memory in macaque prefrontal cortex. Cereb Cortex 2003, 13: 1196–1207.
21. Lucchetti C, Ulrici A, Bon L. Dorsal premotor areas of nonhuman primate: functional flexibility in time domain. Eur J Appl Physiol 2005, 95: 121–130.
22. Mauritz KH, Wise SP. Premotor cortex of the rhesus monkey: neuronal activity in anticipation of predictable environmental events. Exp Brain Res 1986, 61: 229–244.
23. Romo R, Schultz W. Neuronal activity preceding self-initiated or externally timed arm movements in area 6 of monkey cortex. Exp Brain Res 1987, 67: 656–662.
24. Roux S, Coulmance M, Riehle A. Context-related representation of timing processes in monkey motor cortex. Eur J Neurosci 2003, 18: 1011–1016.
25. Lebedev MA, O'Doherty JE, Nicolelis MA. Decoding of temporal intervals from cortical ensemble activity. J Neurophysiol 2008, 99: 166–186.
26. Janssen P, Shadlen MN. A representation of the hazard rate of elapsed time in macaque area LIP. Nat Neurosci 2005, 8: 234–241.
27. Leon MI, Shadlen MN. Representation of time by neurons in the posterior parietal cortex of the macaque. Neuron 2003, 38: 317–327.
28. Schall JD. Neural basis of deciding, choosing and acting. Nat Rev Neurosci 2001, 2: 33–42.
29. Crowe DA, Zarco W, Bartolo R, Merchant H. Dynamic representation of the temporal and sequential structure of rhythmic movements in the primate medial premotor cortex. J Neurosci 2014, 34: 11972–11983.
30. Perez H, Cordova-Fraga T, Lopez-Briones S, Martinez-Espinosa JC, Rosas EF, Espinoza A*, et al.* Portable device for magnetic stimulation: assessment survival and proliferation in human lymphocytes. Rev Sci Instrum 2013, 84: 094701.
31. Merchant H, Perez O, Bartolo R, Mendez JC, Mendoza G, Gamez J*, et al.* Sensorimotor neural dynamics during isochronous tapping in the medial premotor cortex of the macaque. Eur J Neurosci 2015, 41: 586–602.
32. Mello GB, Soares S, Paton JJ. A scalable population code for time in the striatum. Curr Biol 2015, 25: 1113–1122.
33. Gouvea TS, Monteiro T, Motiwala A, Soares S, Machens C, Paton JJ. Striatal dynamics explain duration judgments. Elife 2015, 4.e11386
34. Merchant H, Bartolo R, Pérez O, Méndez JC, Mendoza G, Gámez J*, et al.* Neurophysiology of timing in the hundreds of milliseconds: multiple layers of neuronal clocks in the medial premotor areas. Adv Exp Med Biol 2014, 829: 143–154.
35. Wright BA, Buonomano DV, Mahncke HW, Merzenich MM. Learning and generalization of auditory temporal-interval discrimination in humans. J Neurosci 1997, 17: 3956–3963.
36. Bartolo R, Merchant H. Learning and generalization of time production in humans: rules of transfer across modalities and interval durations. Exp Brain Res 2009, 197: 91–100.
37. Merchant H, Grahn J, Trainor L, Rohrmeier M, Fitch WT. Finding the beat: a neural perspective across humans and non-human primates. Philos Trans R Soc Lond B Biol Sci 2015, 370: 20140093.
38. Fujioka T, Trainor LJ, Large EW, Ross B. Beta and gamma rhythms in human auditory cortex during musical beat processing. Ann N Y Acad Sci 2009, 1169: 89–92.
39. Iversen JR, Repp BH, Patel AD. Top-down control of rhythm perception modulates early auditory responses. Ann N Y Acad Sci 2009, 1169: 58–73.
40. Fujioka T, Trainor LJ, Large EW, Ross B. Internalized timing of isochronous sounds is represented in neuromagnetic beta oscillations. J Neurosci 2012, 32: 1791–1802.
41. Fujioka T, Ross B, Trainor LJ. Beta-band oscillations represent auditory beat and its metrical hierarchy in perception and imagery. J Neurosci 2015, 35: 15187–15198.
42. Merchant H, Bartolo R, Perez O, Mendez JC, Mendoza G, Gamez J*, et al.* Neurophysiology of timing in the hundreds of milliseconds: multiple layers of neuronal clocks in the medial premotor areas. Adv Exp Med Biol 2014, 829: 143–154.
43. Wiener M, Turkeltaub PE, Coslett HB. Implicit timing activates the left inferior parietal cortex. Neuropsychologia 2010, 48: 3967–3971.
44. Ma C, Ma X, Fan J, He J. Neurons in primary motor cortex encode hand orientation in a reach-to-grasp task. Neurosci Bull 2017, 33: 383–395.
45. Bremner LR, Andersen RA. Temporal analysis of reference frames in parietal cortex area 5d during reach planning. J Neurosci 2014, 34: 5273–5284.
46. Reed JL, Pouget P, Qi HX, Zhou Z, Bernard MR, Burish MJ*, et al.* Widespread spatial integration in primary somatosensory cortex. Proc Natl Acad Sci U S A 2008, 105: 10233–10237.
47. Seelke AM, Padberg JJ, Disbrow E, Purnell SM, Recanzone G, Krubitzer L. Topographic maps within brodmann's area 5 of macaque monkeys. Cereb Cortex 2012, 22: 1834–1850.
48. Wang L, Li X, Hsiao SS, Bodner M, Lenz F, Zhou YD. Behavioral choice-related neuronal activity in monkey primary somatosensory cortex in a haptic delay task. J Cogn Neurosci 2012, 24: 1634–1644.
49. Zhang P, Ma X, Chen L, Zhou J, Wang C, Li W*, et al.* Decoder calibration with ultra small current sample set for intracortical brain-machine interface. J Neural Eng 2018, 15: 026019.
50. Bokil H, Andrews P, Kulkarni JE, Mehta S, Mitra PP Chronux a platform for analyzing neural signals. J Neurosci Methods 2010, 192: 146–151.
51. Kilavik BE, Ponce-Alvarez A, Trachel R, Confais J, Takerkart S, Riehle A. Context-related frequency modulations of macaque motor cortical LFP beta oscillations. Cereb Cortex 2012, 22: 2148–2159.
52. Kilavik BE, Zaepffel M, Brovelli A, MacKay WA, Riehle A. The ups and downs of beta oscillations in sensorimotor cortex. Exp Neurol 2013, 245: 15–26.
53. Kilavik BE, Confais J, Riehle A. Signs of timing in motor cortex during movement preparation and cue anticipation. Adv Exp Med Biol 2014, 829: 121–142.
54. Pfurtscheller G, Lopes da Silva FH. Event-related EEG/MEG synchronization and desynchronization: basic principles. Clin Neurophysiol 1999, 110: 1842–1857.
55. Pfurtscheller G, Neuper C, Andrew C, Edlinger G. Foot and hand area mu rhythms. Int J Psychophysiol 1997, 26: 121–135.

56. Pfurtscheller G, Neuper C. Motor imagery activates primary sensorimotor area in humans. Neurosci Lett 1997, 239: 65–68.
57. Kuhn AA, Williams D, Kupsch A, Limousin P, Hariz M, Schneider GH, *et al.* Event-related beta desynchronization in human subthalamic nucleus correlates with motor performance. Brain 2004, 127: 735–746.
58. Lee JH, Whittington MA, Kopell NJ. Top-down beta rhythms support selective attention via interlaminar interaction: a model. PLoS Comput Biol 2013, 9: e1003164.
59. Kopell N, Ermentrout GB, Whittington MA, Traub RD. Gamma rhythms and beta rhythms have different synchronization properties. Proc Natl Acad Sci U S A 2000, 97: 1867–1872.
60. Deiber MP, Missonnier P, Bertrand O, Gold G, Fazio-Costa L, Ibanez V, *et al.* Distinction between perceptual and attentional processing in working memory tasks: a study of phase-locked and induced oscillatory brain dynamics. J Cogn Neurosci 2007, 19: 158–172.
61. Siegel M, Warden MR, Miller EK. Phase-dependent neuronal coding of objects in short-term memory. Proc Natl Acad Sci U S A 2009, 106: 21341–21346.
62. Bartolo R, Prado L, Merchant H. Information processing in the primate basal ganglia during sensory-guided and internally driven rhythmic tapping. J Neurosci 2014, 34: 3910–3923.
63. 63. Baddeley A. Working memory: theories, models, and controversies. Annu Rev Psychol 2012, 63: 1–29.
64. Halsband U, Lange RK. Motor learning in man: a review of functional and clinical studies. J Physiol Paris 2006, 99: 414–424.
65. Miyachi S, Hirata Y, Inoue K, Lu X, Nambu A, Takada M. Multisynaptic projections from the ventrolateral prefrontal cortex to hand and mouth representations of the monkey primary motor cortex. Neurosci Res 2013, 76: 141–149.
66. Tomasino B, Gremese M. The cognitive side of M1. Front Hum Neurosci 2016, 10: 298.
67. Rossi-Pool R, Salinas E, Zainos A, Alvarez M, Vergara J, Parga N, *et al.* Emergence of an abstract categorical code enabling the discrimination of temporally structured tactile stimuli. Proc Natl Acad Sci U S A 2016, 113: E7966–E7975.
68. Zhao D, Zhou YD, Bodner M, Ku Y. The causal role of the prefrontal cortex and somatosensory cortex in tactile working memory. Cereb Cortex 2017, 28: 1–10.
69. Gogulski J, Zetter R, Nyrhinen M, Pertovaara A, Carlson S. Neural substrate for metacognitive accuracy of tactile working memory. Cereb Cortex 2017, 27: 5343–5352.
70. Murray JD, Jaramillo J, Wang XJ. Working memory and decision-making in a frontoparietal circuit model. J Neurosci 2017, 37: 12167–12186.
71. Pisella L. Visual perception is dependent on visuospatial working memory and thus on the posterior parietal cortex. Ann Phys Rehabil Med 2017, 60: 141–147.
72. Birba A, Hesse E, Sedeno L, Mikulan EP, Garcia MDC, Avalos J, *et al.* Enhanced working memory binding by direct electrical stimulation of the parietal cortex. Front Aging Neurosci 2017, 9: 178.
73. 73. Martinez-Vazquez P, Gail A. Directed interaction between monkey premotor and posterior parietal cortex during motor-goal retrieval from working memory. Cereb Cortex 2018, 28: 1866–1881.
74. Engel AK, Fries P. Beta-band oscillations–signalling the status quo? Curr Opin Neurobiol 2010, 20: 156–165.
75. Zhang YY, Xu L, Liang ZY, Wang K, Hou B, Zhou Y, *et al.* Separate neural networks for gains and losses in intertemporal choice. Neurosci Bull 2018, 34: 725–735.
76. Dotson NM, Hoffman SJ, Goodell B, Gray CM. A large-scale semi-chronic microdrive recording system for non-human primates. Neuron 2017, 96: 769–782 e762.
77. Barnett L, Seth AK. The MVGC multivariate granger causality toolbox: a new approach to granger-causal inference. J Neurosci Methods 2014, 223: 50–68.
78. Sheikhattar A, Miran S, Liu J, Fritz JB, Shamma SA, Kanold PO, *et al.* Extracting neuronal functional network dynamics via adaptive Granger causality analysis. Proc Natl Acad Sci USA 2018, 115: E3869–E3878.